Journal of Alloys and Compounds 509 (2011) 7749–7757

Contents lists available at ScienceDirect

Journal of Alloys and Compounds

journal homepage: www.elsevier.com/locate/jallcom

# Effects of Pd concentration on the interfacial reaction and mechanical reliability of the Sn–Pd/Ni system

Cheng-En Ho*, Sheng-Wei Lin, Yen-Chen Lin

*Department of Chemical Engineering & Materials Science, Yuan Ze University, Chungli city, Taiwan, ROC*

ARTICLE INFO

*Article history:*
Received 17 February 2011
Received in revised form 27 April 2011
Accepted 30 April 2011
Available online 10 May 2011

*Keywords:*
Pd concentration effects
Sn–Pd/Ni
$(Pd,Ni)Sn_4$
$Ni_3Sn_4$
HSBS

ABSTRACT

The liquid–solid reaction between Sn–*x*Pd alloy and Ni ($x = 0.05$–1 wt.%) and the resulting mechanical reliability of the system were examined in this study. The reactions strongly depended on the Pd concentration and the reaction time. When the Pd concentration was low (i.e., $x = 0.05$ wt.%), the reaction product was only $Ni_3Sn_4$. In contrast, when the Pd concentration was high (i.e., $x \geq 0.2$ wt.%), the reaction product became a dual-layer structure of $(Pd,Ni)Sn_4$–$Ni_3Sn_4$. Between 0.05 wt.% and 0.2 wt.% (e.g., $x = 0.1$ wt.%), discontinuous $(Pd,Ni)Sn_4$ grains scattered over the $Ni_3Sn_4$ layer developed. Interestingly, the $(Pd,Ni)Sn_4$ grains were gradually dispersed in the molten Sn–Pd alloy, leaving the $Ni_3Sn_4$ at the interface, as the reaction time increased. These Pd-dependent reactions were dictated by thermodynamics and can be rationalized using the Pd–Ni–Sn isotherm. Furthermore, the results of the high-speed-ball-shear (HSBS) test indicated that the mechanical strength of the Sn–Pd/Ni joints dramatically degraded by over one third due to the formation of $(Pd,Ni)Sn_4$ at the interface. The implication is that the Pd concentration in Sn–Pd solder joints should be reduced to a level below 0.2 wt.% to prevent the creation of an undesired microstructure.



## 1. Introduction

Palladium-on-Ni(P) surface finishes, such as Pd/Ni(P) or Au/Pd/Ni(P), have recently received a great deal of attention in the microelectronics industry due to their low cost and high reliability in both wire-bonding and soldering applications [1,2]. In terms of soldering applications, the Ni(P) layer provides a good diffusion barrier between the solder and Cu trace, retarding pad consumption/intermetallic growth [3]. The surface Au serves as a protective layer against the oxidation of the Ni(P) finish. The insertion of a Pd (or Pd–P) film between Au and Ni(P) improves the wettability and acts as a diffusion barrier as well [4,5]. Additionally, the Pd film prevents the Ni(P) from the galvanic hyper-corrosion caused by the Au displacement reaction, thereby reducing the concern of "black pads" [1,6,7]. The thicknesses of the Au and Ni(P) deposited are customarily less than 0.1 μm and more than 5 μm, respectively, but that of the Pd layer has not yet been specified. The Pd film is preliminary deposited within the range of 0.05–0.3 μm (thickness) based on cost-effectiveness [1,8]. During soldering, the Pd layer quickly alloys with the molten solder at an early stage of soldering after the surface Au is exhausted [9–11]. After the entire Pd layer is removed from the interface, the underlying Ni (or Ni–P) comes into contact with a solder containing various Pd concentrations, depending on the Pd thickness and joint dimensions.

The effect of the Pd concentration on the reaction between Ni and Sn–Pd alloys (Pd concentrations: 1, 3, and 5 at.%) at temperatures of 180 °C and 200 °C has been examined by Masui and Kajihara [12]. This reaction refers to a solid–solid reaction between Ni and Sn–Pd, which is a two-phase alloy consisting of β-Sn and $PdSn_4$ [13]. It was found that the $PdSn_4$ gradually migrates from the Sn matrix to the Sn–Pd/Ni interface during the solid-state reaction, enhancing the overall thickness ($\delta$) of the reaction products. The $\delta$ follows a parabolic relationship with the reaction time, i.e., $\delta = kt^{0.5}$, where the growth coefficient $k$ is one order of magnitude larger for 1–5% Pd than for 0% Pd. Thus, the Pd (or $PdSn_4$) has a significant influence on the reaction kinetics between the solid Ni and the solid Sn–Pd alloy [12].

The soldering reaction between Ni and Sn–Pd alloys at 250 °C was recently studied by Ho et al. [14]. The reaction refers to a solid–liquid reaction in which the Ni is a solid but the Sn–Pd alloy becomes a liquid (or paste), unlike that examined by Masui and Kajihara [12]. It was found that the solid–liquid reaction is much more sensitive to the Pd concentration, even with variations in concentration as low as 0.1 wt.%. At a low Pd concentration (e.g., 0.05 wt.%), only a layer of $Ni_3Sn_4$ grew at the interface. At a medium Pd concentration (e.g., 0.05–0.2 wt.%), a layer of $Ni_3Sn_4$ along with discontinuous $(Pd,Ni)Sn_4$ grains coexisted at the interface. At a high

* Corresponding author at: Department of Chemical Engineering & Materials Science, Yuan Ze University, Taoyuan 320, Taiwan, ROC. Tel.: +886 3 4638800x3552; fax: +886 3 4559373.
*E-mail address:* ceho1975@hotmail.com (C.-E. Ho).

0925-8388/$ – see front matter © 2011 Elsevier B.V. All rights reserved.
doi:10.1016/j.jallcom.2011.04.142

Pd concentration (e.g., 0.2–0.5 wt.%), the (Pd,Ni)$Sn_4$ grew as a layer over the $Ni_3Sn_4$. The Pd-dependent reaction is dictated by thermodynamics, and the details have been reported elsewhere in the literature [14].

In the aforementioned study [14], however, only one reaction time (120 s) within a narrow Pd concentration range (0.05–0.5 wt.%) was investigated. Results of the reaction at various times and high Pd concentrations are still quite lacking. The purpose of this study was to establish a more complete database, in which more reaction times (30–1200 s) and Pd concentrations (0.05–1 wt.%) are included, to provide a better understanding of the effect of the Pd concentration on the reaction between solid Ni and liquid Sn–Pd. Additionally, mechanical response of the Sn–Pd/Ni system was also investigated through a high-speed-ball-shear (HSBS) test.

## 2. Experimental details

The soldering reaction between Sn–*x*Pd alloy and Ni, and the mechanical properties of the resulting Sn–*x*Pd/Ni joints were examined in this study. The Ni was deposited over a 375-μm ($d_{pad}$) Cu pad by electroplating (Fig. 1), thereby making it free of P or V. The thickness of the Ni layer was about 7 μm and was not depleted during the soldering reaction. The Sn–*x*Pd alloy was prepared from 99.99% pure Sn and 99.95% pure Pd, where *x* is 0.05, 0.1, 0.2, 0.3, 0.5, 0.7, and 1 wt.%, respectively. Each alloy was sealed in an evacuated quartz tube ($5 \times 10^{-3}$ Torr), mixed in a furnace setup at 900 °C for 3 days, and then quenched in water. The alloys were cross-sectioned before use, metallographically polished to ensure homogeneity, and subsequently shaped into solder balls with a diameter of 1200 μm ($d_{joint}$). These solder balls were then planted onto individual pads, and at least fifteen solder joints were made for each solder composition and reaction time. Before the reaction, each pad was etched by a 30% $HNO_3$ aqueous solution and then smeared with a RMA (rosin mildly activated) flux to remove oxidized contaminations.

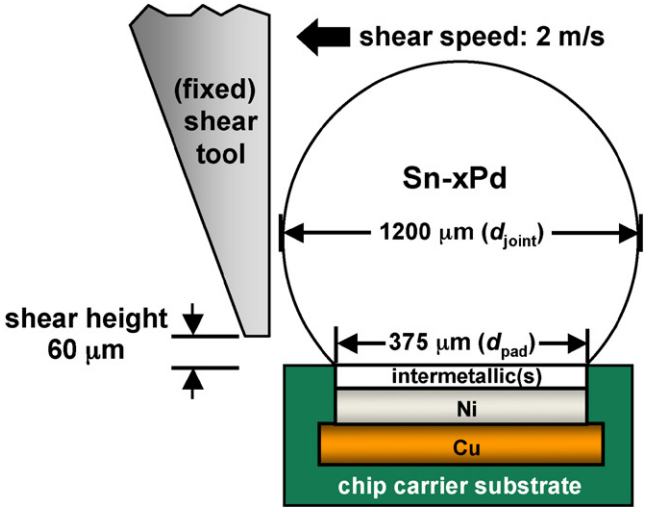


**Fig. 1.** Schematic diagram of a Sn–*x*Pd solder joint under the high-speed-ball-shear (HSBS) test. A shear speed of 2 m/s was applied in shearing.

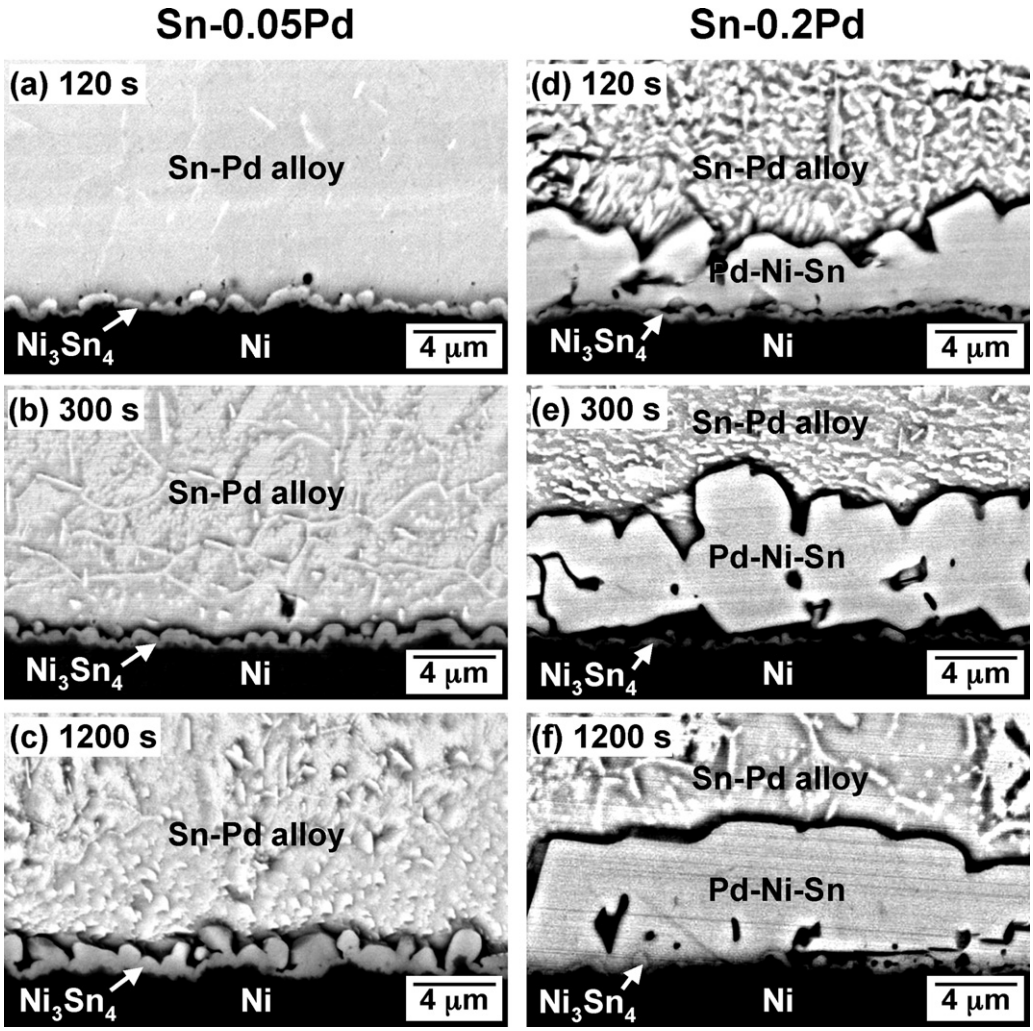


**Fig. 2.** Backscattered electron images (BEI) showing the Sn–*x*Pd/Ni interfaces after reacting at 250 °C for 120 s (a and d), 300 s (b and e), and 1200 s (c and f). The *x* values were 0.05 (a–c) and 0.2 (d–f), respectively.

The soldering reaction was carried out at 250 °C for 30–1200 s. After the reaction, the solder joints were immediately quenched in water. A batch of solder joints was then cross-sectioned by a metallographical grinding–polishing process to reveal the detailed microstructures of the joints. The composition of each reaction product was determined by a field-emission electron probe micro-analyzer (FE-EPMA) operated at 12 keV. Such a low accelerated voltage produced a much smaller interaction volume between the incident electron beam and the measured specimen than that created by the traditional mode; thus, compositional measurements of some minute phases were possible. Additionally, a field-emission transmission electron microscopy (FE-TEM) (type: JEM-2100F) operated at 200 keV was employed to identify the crystal structures of the reaction products. The specimens for TEM examination were prepared using a focused ion beam (FIB) apparatus.

To evaluate the effect of the Pd concentration on the mechanical properties, another batch of solder joints was examined via the HSBS test. The shear test was carried out using a bond tester (type: DAGE 4000HS) according to the JESD22-B117 specification [15]. The shear speed and shear height were set to 2 m/s and 60 μm (Fig. 1), respectively. For each data point, at least ten measurements were made, and the average value was reported. The fracture surfaces of the solder joints after the HSBS test were examined using scanning electron microscopy-energy dispersive X-ray spectroscopy (SEM-EDX). Additionally, a micro X-ray photoelectron spectroscopy (μ-XPS) with a spot size of about 9 μm was employed to pinpoint the exact position of the fracture.

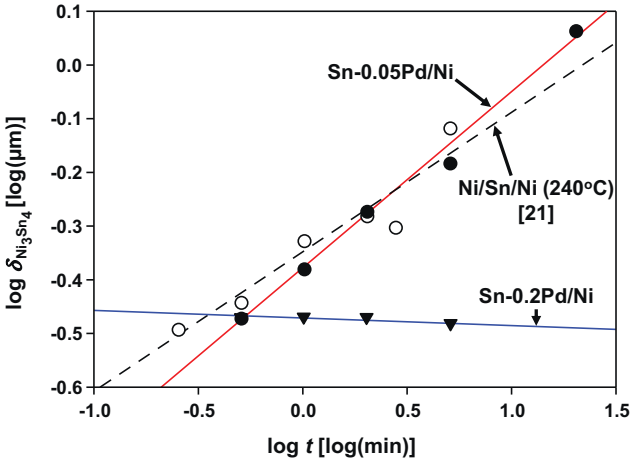


**Fig. 3.** Growth of the $Ni_3Sn_4$ phase in the Sn–0.05Pd/Ni, Sn–0.2Pd/Ni, and Ni/Sn/Ni reactions. The data of the Ni/Sn/Ni system (broken line) is adapted from the work of Bader et al. [21] and re-plotted in this study.

## 3. Results

### 3.1. Low Pd-concentration case ($x$ = 0.05, 0.1, 0.2, and 0.3)

Fig. 2 shows the cross-section of the Sn–$x$Pd/Ni interfaces ($x$ = 0.05 and 0.2) that were reacted at 250 °C for 120 s (a and d), 300 s (b and e), and 1200 s (c and f). A clear trend in these reactions is that the amount of the reaction product(s) at the interface increased with the reaction time as well as the Pd concentration. Moreover, the type of reaction product produced is strongly dependent on $x$, even with a concentration differences as small as 0.15 wt.%.

The Sn–0.05Pd/Ni reaction produced a scallop-like compound layer at the interface for all of the times examined, as shown in Fig. 2a–c. With the aid of FE-EPMA, the compound was identified as $Ni_3Sn_4$, with a very limited amount of Pd (~0.2 at.%) dissolved in it. The formation of intermetallic $Ni_3Sn_4$ at the interface is consistent with the soldering systems of Ni and most Sn-based alloys [16,17], excluding reactions alloying with additional active elements such as Cu [16,18] or Zn [19,20]. The type of reaction product ($Ni_3Sn_4$) observed did not change over time, but the thickness ($\delta_{Ni_3Sn_4}$) varied (Fig. 2a–c). Fig. 3 is a plot of $\log\delta_{Ni_3Sn_4} - \log t$, which provides a further illustration of the Pd effect on the $Ni_3Sn_4$ growth behavior. The $\delta_{Ni_3Sn_4}$ was measured using electron micrographs and a calibrated image analysis software. The thickness is defined as the phase area divided by a linear length of the interface. In the case of the Sn–0.05Pd/Ni reaction (red line), the r-square value is approximately 0.99, indicating that the measured data are closely fitted by linear regression. The slope and intercept values computed from the red line were 0.33 and −0.38, respectively. Accordingly, the growth thickness of $Ni_3Sn_4$ in this case (i.e., Sn–0.05Pd/Ni) increased linearly as a function of $0.42t^{0.33}$. This observation suggests that the growth kinetics of $Ni_3Sn_4$ for the Sn–0.05Pd/Ni reaction is dominated by neither the diffusion-controlled mechanism nor the reaction-controlled mechanism. This growth behavior is very similar to that of $\delta_{Ni_3Sn_4} = 0.45t^{0.28}$ (as the broken line in Fig. 3) reported in the literature [21], where a thin Ni/Sn/Ni diffusion couple was utilized and a short-circuit diffusion mechanism was proposed to be the root cause of the unique growth [17]. The results above indicate

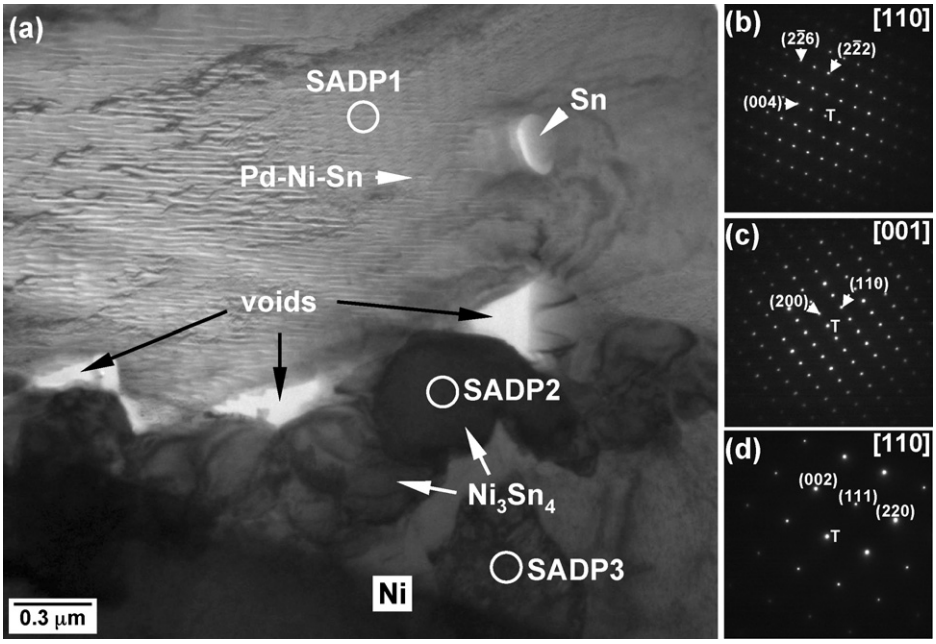


**Fig. 4.** (a) TEM bright field image of the Sn–0.2Pd/Ni interface after reacting at 250 °C for 120 s. (b–d) Selected-area diffraction patterns (SADPs) from $(Pd,Ni)Sn_4$ (SADP1), $Ni_3Sn_4$ (SADP2), and Ni (SADP3), respectively.

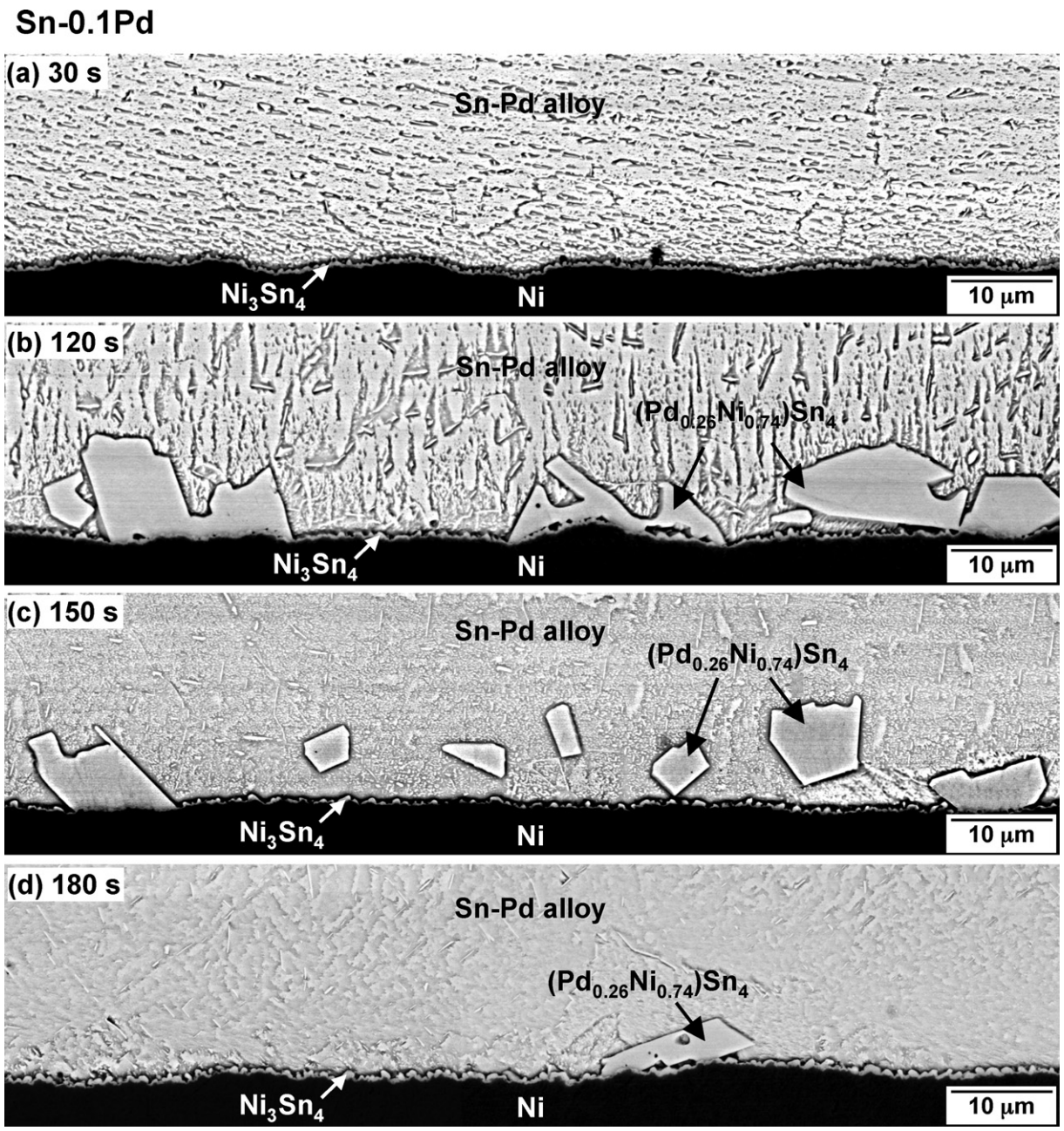


**Fig. 5.** Backscattered electron images showing the Sn–0.1Pd/Ni interfaces after reacting at 250 °C for 30 s (a), 120 s (b), 150 s (c), and 180 s (d).

that the addition of 0.05 wt.% Pd has a minor effect on the soldering reaction between Ni and Sn.

In contrast, there were two adjacent compound layers that nucleated at the interface when $x$ increased to 0.2 (Fig. 2d–f). The layer neighboring the Ni was extremely thin and was identified using FE-EPMA as $Ni_3Sn_4$, as was obtained in the Sn–0.05Pd/Ni case. Interestingly, the thickness of the $Ni_3Sn_4$ layer did not increase with the reaction time but remained approximately the same at all times examined (Fig. 2d–f and Fig. 3). A further discussion of this unique growth mechanism is given in the subsequent section (Section 4.2).

The second layer, which grew between $Ni_3Sn_4$ and the Sn–Pd alloy, was much thicker than $Ni_3Sn_4$, as shown in Fig. 2d–f. The composition was determined using EPMA to be 7.7–8.9 at.% Pd, 10.9–14.3 at.% Ni, and 78.4–80.2 at.% Sn, which deviates from all of the possible intermetallics existed in the Ni–Sn binary system, e.g., $Ni_3Sn$, $Ni_3Sn_2$, and $Ni_3Sn_4$. The formation of this Pd–Ni–Sn compound is not a transient phenomenon and can persist for at least 1200 s (Fig. 2f). The progressive growth of the Pd–Ni–Sn layer, as shown in Fig. 2d–f, indicates that the phase was produced when the Ni contacted the molten Sn–0.2Pd alloy, rather than at the stage of solidification. In other words, the Pd–Ni–Sn compound layer was not a product derived from precipitation due to the solubility limit.

Fig. 4 shows a TEM micrograph of the Sn–0.2Pd/Ni interface, together with selected-area diffraction patterns (SADPs). From top to bottom, the layers are Pd–Ni–Sn, $Ni_3Sn_4$, and Ni phases. The Sn–Pd alloy is above the Pd–Ni–Sn layer and is not shown in Fig. 4. The Pd–Ni–Sn phase has the $PdSn_4$-based crystal structure, as evidenced by the SADP shown in Fig. 4b, which agrees well with the EBSD results obtained in the literature [14]. Further examination using TEM-EDX shows that the Pd–Ni–Sn has a composition of 7.3 at.% Pd–13.1 at.% Ni–79.6 at.% Sn (average), which approximates the measurements made via EPMA. This composition was

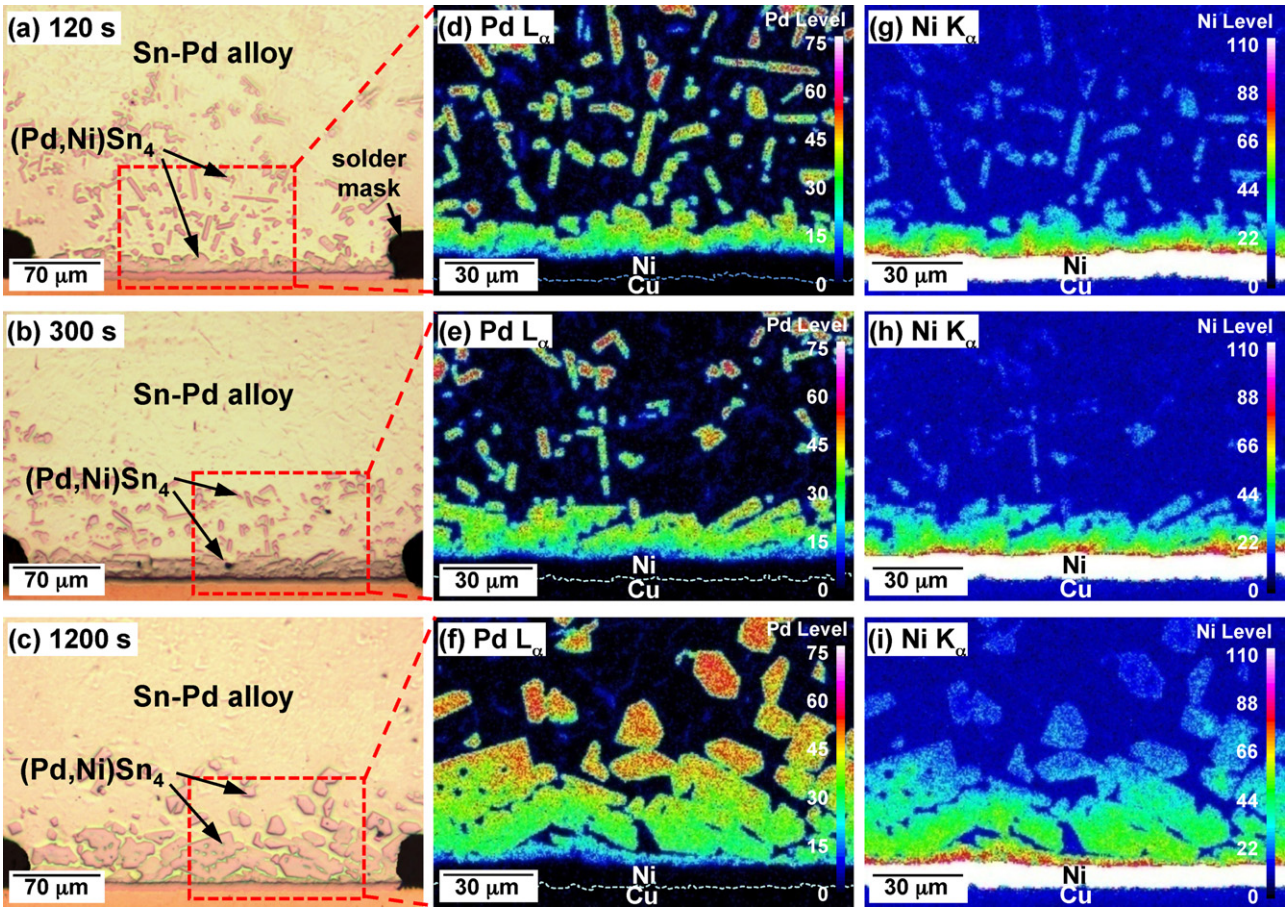


**Fig. 6.** (a–c) Optical micrographs showing the reaction zones between Sn–0.5Pd and Ni after reacting at 250 °C for 120 s, 300 s, and 1200 s, respectively. EPMA elemental mappings of Pd (d–f) and Ni (g–i) corresponding to the regions labeled by the squares in (a–c).

also very similar with the phase (i.e., $(Pd_{0.35}Ni_{0.65})Sn_4$) neighboring the Sn–Ni alloy of the Sn–Ni/Pd system [22]. These results show that a significant amount of Ni replaced the Pd sublattice sites of the $PdSn_4$ crystal. Accordingly, the Pd–Ni–Sn compound should more accurately be referred to as the $(Pd,Ni)Sn_4$ stoichiometry. Immediately adjacent to the $(Pd,Ni)Sn_4$ phase was a $Ni_3Sn_4$ layer with grain sizes of ~0.4 μm (Fig. 4a and c). Additionally, there was a chain of voids that appeared between $Ni_3Sn_4$ and $(Pd,Ni)Sn_4$, which has not been observed at the Sn–0.05Pd/Ni interface. Beneath $Ni_3Sn_4$ was a crystalline Ni metallization pad (Fig. 4a and d). This crystalline rather than amorphous structure reflects the fact that the Ni pads of this study were deposited by electroplating instead of electroless-plating.

When the Pd concentration was between 0.05 wt.% and 0.2 wt.%, e.g., 0.1 wt.%, the type of reaction product produced became time-dependent, as shown in Fig. 5a–d. At 30 s, there was only one compound layer $Ni_3Sn_4$ nucleated at the Sn–0.1Pd/Ni interface (Fig. 5a). At 60 s or 120 s, one additional $(Pd,Ni)Sn_4$ compound with an average composition of $(Pd_{0.26}Ni_{0.74})Sn_4$ appeared at the Sn–0.1Pd/$Ni_3Sn_4$ interface (Fig. 5b). The $(Pd_{0.26}Ni_{0.74})Sn_4$ exhibits a discontinuous, facet-type morphology unlike the layered-type structure produced at the Sn–0.2Pd/Ni interface (Fig. 2d–f). By prolonging the reaction time to 150 s, the amount of $(Pd_{0.26}Ni_{0.74})Sn_4$ present was reduced due to the fact that part of the $(Pd,Ni)Sn_4$ grains spalled into the solder (Fig. 5c). At 180 s, most of the $(Pd_{0.26}Ni_{0.74})Sn_4$ grains disappeared, but the $Ni_3Sn_4$ layer survived (Fig. 5d). Consequently, the overall thickness of the reaction product(s), i.e. $(Pd,Ni)Sn_4$ and $Ni_3Sn_4$, did not always increase over time in the case of Sn–0.1Pd; instead, it increased first (Fig. 5a and b) and then decreased gradually (Fig. 5c and d).

### 3.2. High Pd-concentration case ($x \geq 0.5$)

Fig. 6 shows optical micrographs together with EPMA elemental mappings of the Sn–0.5Pd/Ni interface after reacting for 120 s (a, d and g), 300 s (b, e and h), and 1200 s (c, f and i). These micrographs are representative of the high Pd-concentration case subsequently. The most remarkable difference from the Sn–0.2Pd case (Fig. 2d–f) is that two distinct $(Pd,Ni)Sn_4$ layers existed as $x$ increased to 0.5. At the interface, the $(Pd,Ni)Sn_4$ layer was irregular and much thicker than that obtained in the low Pd-concentration case. Beneath the $(Pd,Ni)Sn_4$ layer, there was a very thin $Ni_3Sn_4$ layer such as that grew in the Sn–0.2Pd/Ni case (Fig. 2d–f). However, the space between $(Pd,Ni)Sn_4$ and $Ni_3Sn_4$ was occupied by the solder, unlike the voiding mentioned above (Fig. 2d–f and Fig. 4). The region in the solder matrix neighboring the interface was a two-phase mixture layer composed of solder and an aggregate of isolated $(Pd,Ni)Sn_4$ domains. The thickness of the $(Pd,Ni)Sn_4$ at the interface increased, but the extent of the two-phase layer of $(Pd,Ni)Sn_4$ + solder reduced as a function of the reaction time.

Another interesting finding is that the composition of the $(Pd,Ni)Sn_4$ varied with location. The EPMA elemental mappings presented in Fig. 6d–i clearly show that the Pd content of the $(Pd,Ni)Sn_4$ increases progressively from the interface towards the solder region (d–f), whereas the Ni concentration shows the opposite trend (g–i). The Ni concentration of the $(Pd,Ni)Sn_4$ reached

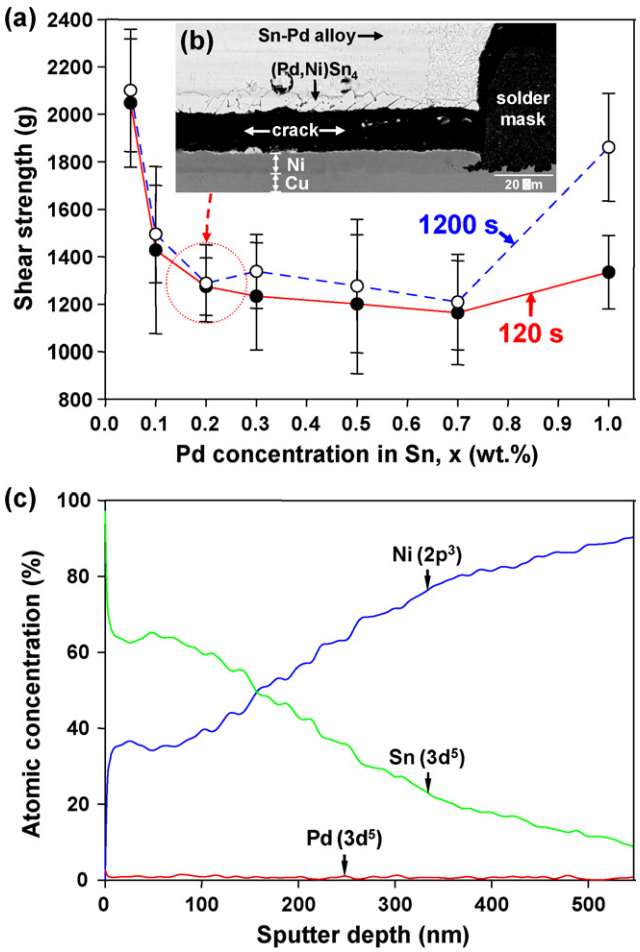


**Fig. 7.** (a) Shear strength of the Sn–*x*Pd/Ni joints as a function of Pd concentration (*x*). (b) Typical fracture of a Sn–0.2Pd/Ni joint after the shear test. (c) μ-XPS depth profiles of the atomic concentrations of the board-side fracture surface for the Sn–0.2Pd/Ni joint after the HSBS test.

a relatively high level of 13.1 at.% (average) at the interface, i.e. $(Pd_{0.34}Ni_{0.66})Sn_4$, which is one order of magnitude larger than that distributed away from the interface. The growth of the high Ni-containing $(Pd_{0.34}Ni_{0.66})Sn_4$ layer at the expense of the low Ni-containing $(Pd,Ni)Sn_4$ domains scattered in the Sn matrix suggests that the phase tends to become more Ni-bearing, i.e., $(Pd_{0.34}Ni_{0.66})Sn_4$.

### 3.3. High-speed-ball-shear test

To quantify mechanical response of the various interfacial microstructures derived from different Pd concentrations (*x*), the HSBS test was used. Fig. 7a shows a plot of the shear strength of the Sn–*x*Pd/Ni joints as a function of the Pd concentration after the test. The solid and dashed lines represent the reaction results at 120 s and 1200 s, respectively. These data were obtained using the same experimental conditions, including a shear tool module (3 kg), shear speed (2 m/s), shear height (60 μm), and reaction temperature (250 °C). The shear strengths were approximately independent of the reaction time (i.e., 120 s and 1200 s), which dramatically dropped, leveled off, and then rose with increasing *x*. The highest strength, ~2100 g, was measured at $x = 0.05$. When *x* increased to 0.2–0.7, the value was substantially reduced to 1200–1400 g, which is about 33–43% lower than that of the Sn–0.05Pd case (Fig. 7a). Interestingly, the strength increased at $x = 1$, specifically for the case of the long-term reaction (i.e., 1200 s). All of the solder joints

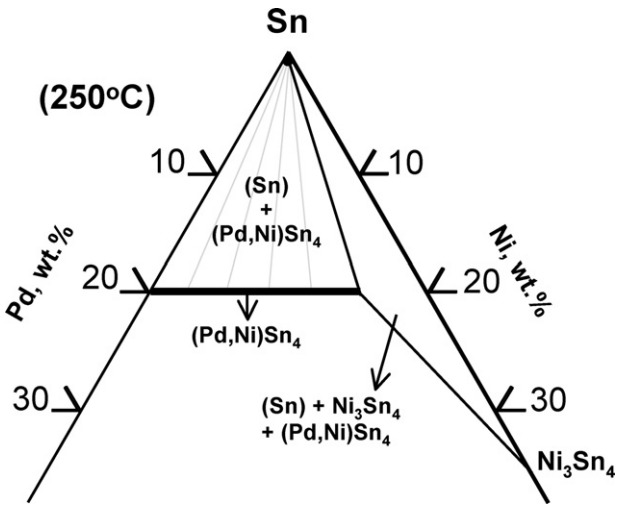


**Fig. 8.** Schematic drawing of the Sn-rich corner of the Pd–Ni–Sn phase diagram at 250 °C. This isotherm was adapted from Ref. [14] and redrawn in this study.

fractured through the Sn–*x*Pd/Ni interface after the HSBS test, with the exception of the Sn–0.05Pd case, where most of the fractures actually occurred either in the solder region or within the substrate. The fracture mode indicates that the formation of a single $Ni_3Sn_4$ phase at the interface has a better resistance against the HSBS impact than the Sn–0.05Pd alloy.

Fig. 7b shows a cross-section of the Sn–0.2Pd/Ni interface after a 120-s reaction and a manual shear test, providing a better understanding of the failure mode of a dense layer of $(Pd,Ni)Sn_4$ formed at the interface. The joint failed approximately through the interface between the $(Pd,Ni)Sn_4$ layer and the Ni substrate, unlike the fracture through the solder region observed in the Sn-0.05/Ni case. To identify a more exact fracture location, a μ-XPS elemental depth profile analysis from the facade of the board-side fracture was performed. In the μ-XPS analysis, the depth scale was defined based on a known $SiO_2$ film that was sputtered by $Ga^+$ ions at an etching rate of 2.1 nm/s. The Sn concentration progressively decreased from about 60 at.%, while the Ni concentration increased from about 40 at.% as a function of the sputtered depth (Fig. 7c). No meaningful Pd signal could be detected from the entire profile, reflecting the fact that the fracture does not occur within the $(Pd,Ni)Sn_4$ layer. The mixture of Ni and Sn extended to a depth of about 500 nm (Fig. 7c), which is comparable to the thickness of the $Ni_3Sn_4$ shown in Fig. 4a. The results of the μ-XPS analysis indicate that the Sn–0.2Pd/Ni joint fails approximately through the $(Pd,Ni)Sn_4/Ni_3Sn_4$ interface.

Interestingly, the fracture translated from the $(Pd,Ni)Sn_4/Ni_3Sn_4$ interface to the $(Pd,Ni)Sn_4$ layer when *x* further increased to 1, providing a possible link between the improved shear strength and the observation of less voiding at the $(Pd,Ni)Sn_4/Ni_3Sn_4$ interface. The combined results of the HSBS test and failure mode suggest that the Pd concentration should be reduced to a level below 0.2 wt.% to prevent the formation of an undesired $(Pd,Ni)Sn_4$ layer at the interface.

## 4. Discussion

### 4.1. Low Pd-concentration case ($x = 0.05$, 0.1, 0.2, and 0.3)

The soldering reaction between Ni and the Sn–*x*Pd alloys strongly depended on the Pd concentration. The reaction product transformed from a single layer of $Ni_3Sn_4$ to a dual layer of $(Pd,Ni)Sn_4$–$Ni_3Sn_4$ as *x* increased from 0.05 to 0.2 (or higher). This Pd-dependent reaction can be rationalized using the Pd–Ni–Sn isotherm (Fig. 8 [14]) as follows. According to Fig. 8, one three-phase

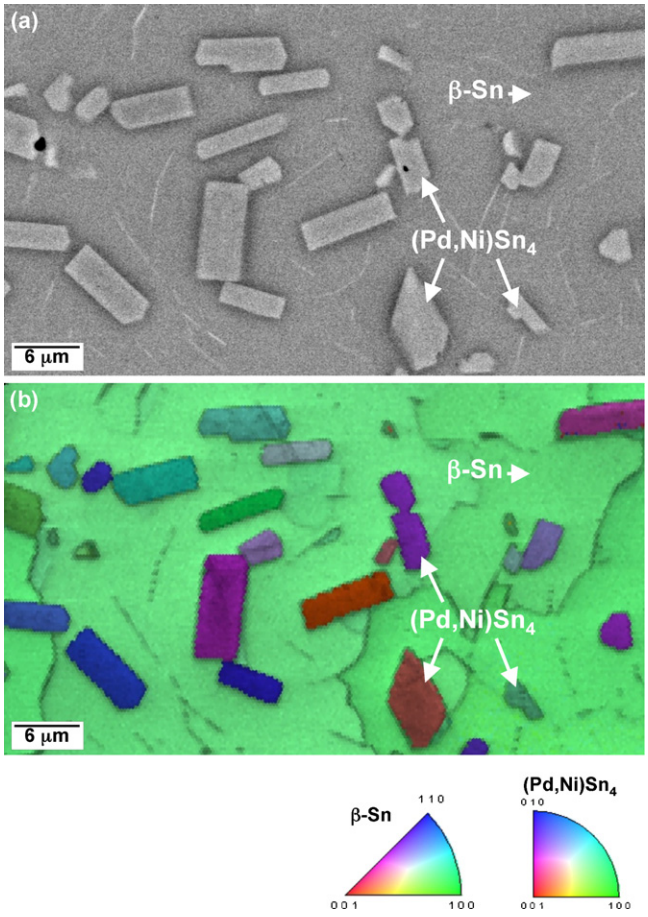


**Fig. 9.** (a) Backscattered electron image showing the solder region near the Sn–0.5Pd/Ni interface that had experienced a 250 °C reaction for 300 s. (b) An EBSD image quality (IQ)-inverse pole figure (IPF) of (a).

field (Sn) + $Ni_3Sn_4$ + $(Pd,Ni)Sn_4$, and two two-phase fields (Sn) + $Ni_3Sn_4$ and (Sn) + $(Pd,Ni)Sn_4$, are in equilibrium with the liquid Sn phase (Sn). The solubility of Pd in both Sn and $Ni_3Sn_4$ is very limited; thus, the two-phase field (Sn) + $Ni_3Sn_4$ is narrow in size and approximates the border of pure Sn + pure $Ni_3Sn_4$. At a low $x$ value (e.g., 0.05), the Sn–Pd alloy represents a tie-line to the $Ni_3Sn_4$, meaning that the formation of the $Ni_3Sn_4$ adjacent to the low Pd-containing alloy is thermodynamically stable. In contrast, as $x$ slightly increased, say to 0.2 wt.%, the growth of a continuous $(Pd,Ni)Sn_4$ phase at the interface became stable because tie-lines existed between the $(Pd,Ni)Sn_4$ and (Sn) containing a relatively high $x$. Thus, the $(Pd,Ni)Sn_4$ and $Ni_3Sn_4$ phases coexisted adjacent to the (Sn) at an intermediate $x$ value (e.g., 0.1) when the three-phase equilibrium (Sn) + $Ni_3Sn_4$ + $(Pd,Ni)Sn_4$, was reached.

In the Sn–0.1Pd/Ni case, however, the $(Pd_{0.26}Ni_{0.74})Sn_4$ grains progressively spalled away from the interface, leaving the $Ni_3Sn_4$ with a limited amount of $(Pd_{0.26}Ni_{0.74})Sn_4$ at the interface after 180 s (Fig. 5). This implies that the formation of both $(Pd_{0.26}Ni_{0.74})Sn_4$ and $Ni_3Sn_4$ at the interface is not stable during a long-term reaction. This time-dependent behavior seems to be contrary to the thermodynamic rationalization explained above. There are two possibilities for this deviation. The first is derived from the Pd concentration drop during the reaction. The $(Pd_{0.26}Ni_{0.74})Sn_4$ clearly grows at the interface at the expense of the Pd within the Sn–Pd alloy. This causes a reduction in the Pd concentration, which might shift the equilibrium relationship from (Sn)–$Ni_3Sn_4$–$(Pd_{0.26}Ni_{0.74})Sn_4$ to (Sn)–$Ni_3Sn_4$ if $x$ is reduced to a low level, say 0.05 (Fig. 8). As a consequence, the coexistence of $Ni_3Sn_4$ and $(Pd_{0.26}Ni_{0.74})Sn_4$ at the interface is destroyed, and an even more stable microstructure, where only the $Ni_3Sn_4$ phase exists at the interface, is established. To validate this assumption, a careful estimation of the Pd concentration drop ($\Delta C_{Pd}$) should be performed.

According to [18,23], the $\Delta C_{Pd}$ under different combinations of pad diameter ($d_{pad}$) and joint diameter ($d_{joint}$) can be expressed as,

$$\Delta C_{Pd} = \frac{3}{2}\left(\frac{d_{pad}^2}{d_{joint}^3}\right)\left(\frac{\rho_{(Pd,Ni)Sn_4}}{\rho_{Sn-Pd}}\right) w_{Pd}\delta_{(Pd,Ni)Sn_4} \quad (1)$$

where $\rho_{(Pd,Ni)Sn_4}$ and $\rho_{Sn-Pd}$ represent the density of $(Pd,Ni)Sn_4$ and the Sn–Pd alloy, respectively. $w_{Pd}$ represents the Pd content of $(Pd,Ni)Sn_4$, and $\delta_{(Pd,Ni)Sn_4}$ represents the $(Pd,Ni)Sn_4$ thickness.

In this study, $d_{pad}$ and $d_{joint}$ are 375 μm and 1200 μm, respectively, as depicted in Fig. 1. $\rho_{(Pd,Ni)Sn_4}$ and $\rho_{Sn-Pd}$ can be taken to be ~8.175 g/cm$^3$ (the density of $PdSn_4$) and ~7.31 g/cm$^3$ (the density of pure Sn), respectively. $w_{Pd}$ and $\delta_{(Pd,Ni)Sn_4}$ for the Sn–0.1Pd/Ni case were measured to be ~5.6 wt.% and ~3.7 μm (average) after a 120-s reaction. Accordingly, the resulting $\Delta C_{Pd}$ is ~0.0028 wt.%, which is two orders of magnitude smaller than the initial Pd concentration (0.1 wt.%). This estimation indicates that the Pd concentration remains approximately the same during the reaction, suggesting that $\Delta C_{Pd}$ might not be a key factor responsible for the microstructural evolution observed in Fig. 5.

An alternative explanation for the disappearance of $(Pd_{0.26}Ni_{0.74})Sn_4$ from the interface is attributed to the fact that the Ni content in (Sn) increases over time. The dissolution of Ni changes the adjacent Sn–0.1Pd alloy into a Ni-containing Sn–0.1Pd alloy, where the (Sn) is locally in equilibrium with the $Ni_3Sn_4$ and $(Pd,Ni)Sn_4$. Therefore, the composition of the Sn–Pd alloy (or the Ni and Pd concentrations) neighboring the interface is different from that of the bulk region. As the reaction time increases, the concentration gradient continues to deliver the Ni atoms to the other region unsaturated with Ni, thereby increasing the extent of the (Sn)–$Ni_3Sn_4$–$(Pd,Ni)Sn_4$ three-phase equilibrium. Accordingly, the $(Pd,Ni)Sn_4$ phase has no need to maintain its stability by attaching itself to the $Ni_3Sn_4$ at the interface; instead, it can grow anywhere with sufficient Ni. The possibility of this alternative mechanism is currently being evaluated using Ni-doping Sn–Pd alloys for the reaction.

Kinetically, intermetallic spalling usually follows the Ostwald ripening process [24,25], in which atoms of the smaller grains are driven to the larger grains due to the concentration gradient that is created via the Gibbs–Thomson effect [26]. The spalling phenomenon reported in [24,25], however, was induced by the exhaustion of the substrate (i.e., Cu); this results in a compound layer (i.e., $Cu_6Sn_5$) that is in direct contact with the oxidized Cr layer, which has poor wettability with $Cu_6Sn_5$. This is unlike the situation encountered in this study, where most of the $(Pd_{0.26}Ni_{0.74})Sn_4$ detaches from the interface, even though the substrate has not yet been exhausted. We proposed the convection of molten solder to be the driving force for the detachment of the unstable $(Pd_{0.26}Ni_{0.74})Sn_4$ grains from the interface (Fig. 5).

### 4.2. High Pd-concentration case ($x \geq 0.5$)

According to the literature [27], the saturation solubility of Pd in Sn–Ag solder at 250 °C (i.e., the reaction temperature used in this study) is about 0.4 wt.%. Assuming that it is compatible with the situation of pure Sn, the high Pd-containing alloys (0.5–1 wt.% Pd) enter the so-called "paste zone", in which the alloys actually consist of liquid Sn and $PdSn_4$ phases. This scenario is distinctly different from its counterpart (i.e., the low Pd-concentration case) in that only one liquid Sn phase survives at 250 °C. In other words, the Pd

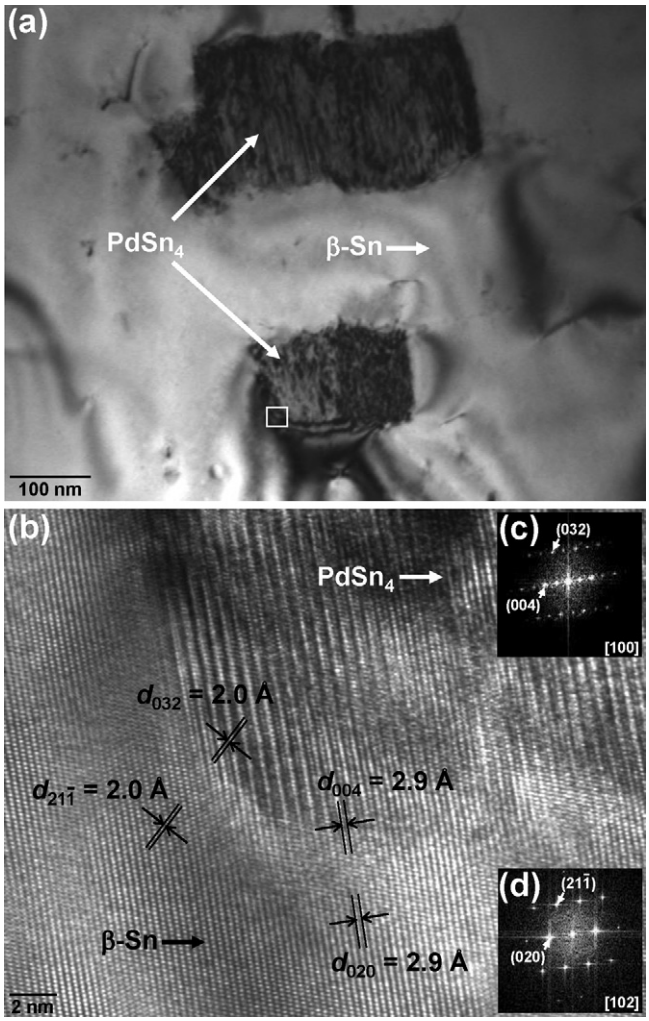


**Fig. 10.** (a) TEM bright field image of the $PdSn_4$ domains in the β-Sn matrix. (b) Magnified image of the area labeled by the square in (a). (c–d) Fast Fourier transform (FFT) obtained from the $PdSn_4$ and β-Sn lattice information provided in (b), respectively.

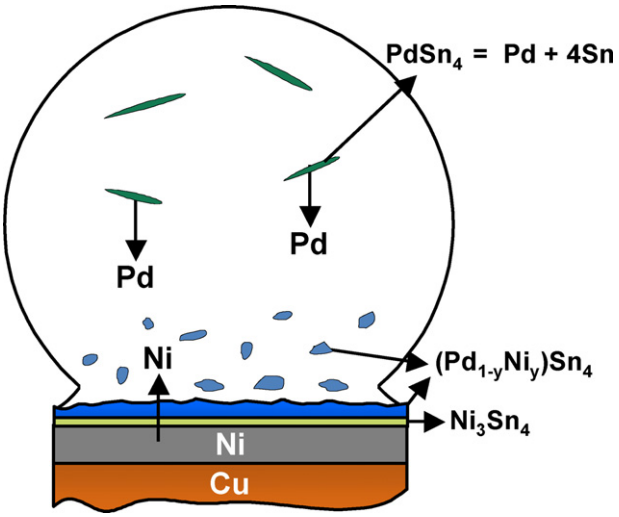


**Fig. 11.** Schematic drawing of the $(Pd_{1-y}Ni_y)Sn_4$ growth mechanism in the high Pd-concentration case.

in the high Pd-concentration alloys exists in the forms of Pd atoms and $PdSn_4$.

During soldering, the dissolution of the Ni substrate transforms the binary Sn–Pd alloy into a ternary Sn–Pd–Ni system, shifting the equilibrium from (Sn)–$PdSn_4$ to (Sn)–(Pd,Ni)$Sn_4$ (Fig. 8). As a result, the *pure* $PdSn_4$ phase is no longer stable but is required to transform itself into a Ni-containing phase, i.e. (Pd,Ni)$Sn_4$, instead. This change drives the $PdSn_4$ grains originally in the (Sn) matrix to migrate towards the interface, to gain Ni from the Ni substrate, shifting to the stable (Pd,Ni)$Sn_4$ phase. The phenomenon wherein the (Pd,Ni)$Sn_4$ grains tend to migrate to the interface and become more Ni-containing phases, as shown in Fig. 6, supports this view.

Fig. 9a and b shows a BEI together with an image produced by electron backscatter diffraction-orientation image microscopy (EBSD-OIM) of the solder region neighboring the interface, providing further information regarding the crystallographic correlation of the (Pd,Ni)$Sn_4$ grains with the solder matrix. The results of EBSD-OIM indicate that the isolated phase domains have the same $PdSn_4$-based crystal structure (FC orthorhombic; space group: *Aba*2) and randomly distribute in the solder matrix, independent of the β-Sn orientation. This incoherent crystallographic relationship shows that the orientations of the scattered (Pd,Ni)$Sn_4$ grains are unrestricted by the Sn matrix during soldering. This lack of restriction in orientation occurs because the crystal structure of β-Sn was destroyed in the molten state. The observation provides a proof of the two-phase mixture layer of (Pd,Ni)$Sn_4$–(Sn) shown in Fig. 6 was well developed during the liquid–solid reaction.

Fig. 9 also reveals that there are many white, strip-like grains uniformly scattered inside the Sn matrix. A similar result can also be observed in Figs. 2, 5 and 6. The thickness of the strip-like grains, however, is too thin for their composition/crystal structure to be accurately measured though FE-EPMA or EBSD (Fig. 9b). According to the Pd–Sn phase diagram [13], the $PdSn_4$ intermetallic is the only phase in equilibrium with the β-Sn when the Pd concentration in a Sn–Pd alloy is less than 20%. It is, therefore, presumed that these tiny grains represent the $PdSn_4$ phase, which form in the solidification stage due to the solubility limit. To further verify this assumption, FE-TEM was employed to identify the crystal structure of the compound and the crystallographic correlation with the β-Sn matrix. Fig. 10a shows a TEM bright-field (BF) image of the solder region after reacting at 250 °C. Two isolated phase domains in the Sn matrix can be clearly observed in this figure. Fig. 10b displays a lattice image of the area neighboring the grain boundary between one of the isolated domain and the β-Sn phase. The insets (Fig. 10c and d) show electron diffraction patterns from the two phases, which were obtained using the lattice image (Fig. 10b) simulated by fast Fourier transform (FFT) through the Gatan DigitalMicrograph software (version 1.83). The lattice information provided in Fig. 10b and c indicates that the isolated grains are indeed based on the $PdSn_4$ crystal structure and that a coherent orientation relationship exists between the $PdSn_4$ phase and the β-Sn matrix:

$$[100]_{PdSn_4}//[102]_{\beta-Sn}, (032)_{PdSn_4}//(21\bar{1})_{\beta-Sn},$$
$$(004)_{PdSn_4}//(020)_{\beta-Sn}$$

This coherent crystallographic correlation suggests that these strip-like $PdSn_4$ grains in the β-Sn matrix (Figs. 2, 5, 6 and 9) are most likely derived from the precipitation during solidification, unlike the growth mechanism of the chunk-like (Pd,Ni)$Sn_4$ grains shown in Fig. 9.

The resettlement of $PdSn_4$ from the solder matrix caused a significant growth of the phase at the interface, especially in the high Pd-concentration case (Fig. 6). The resettlement relies on the Pd atoms diffusing to the interface, instead of an unity of $PdSn_4$, as

shown in Fig. 11. Therefore, the $PdSn_4$ should decompose first according to the following equation:

$$PdSn_4 = Pd + 4Sn \quad (2)$$

The Pd atoms should then diffuse to the interface and react with the $Ni_3Sn_4$ into the Ni-bearing $(Pd_{1-y}Ni_y)Sn_4$, according to Eq. (3):

$$(1-y)Pd + \left(\frac{y}{3}\right) Ni_3Sn_4 + 4\left(1-\left(\frac{y}{3}\right)\right) Sn = (Pd_{1-y}Ni_y)Sn_4 \quad (3)$$

Eq. (3) indicates that the formation of one mole of $(Pd_{1-y}Ni_y)Sn_4$ at the interface requires $y/3$ mole of $Ni_3Sn_4$ and $4(1-y/3)$ mole of Sn. In the case of $x = 0.5$, $y$ is determined to be 0.36; that is, 0.12 mole of $Ni_3Sn_4$ and 3.52 mole of Sn will be depleted when one mole of $(Pd_{0.64}Ni_{0.36})Sn_4$ is produced. This provides a possible explanation as to why the $Ni_3Sn_4$ growth was retarded when a layer of $(Pd,Ni)Sn_4$ nucleated over the $Ni_3Sn_4$ (Figs. 3 and 6). Another explanation is that the $(Pd,Ni)Sn_4$ phase is very thick and continuous, so the atomic interdiffusion is significantly inhibited and the $Ni_3Sn_4$ growth is retarded [28]. The calculated result also shows that a plenty of Sn is depleted in the growth of $(Pd_{0.64}Ni_{0.36})Sn_4$. However, the enormous depletion of Sn did not produce significant voids in the solder matrix (Fig. 6) because the solder was in the molten state during the reaction; thus, any vacancy produced should be filled with the molten solder very quickly.

The growth mechanism of $(Pd,Ni)Sn_4$ aforementioned is quite similar to that of the layered-type $(Au,Ni)Sn_4$ [17,29,30] and $(Cu,Ni)_6Sn_5$ [31,32] developed at the solder/Ni interface, whereas the decomposition of $PdSn_4$ (Eq. (2)) and the diffusion of Pd atoms (Eq. (3)) both occurred in the liquid solder, unlike $AuSn_4$ or $Cu_6Sn_5$ in a solid. Consequently, a much higher growth rate of $(Pd,Ni)Sn_4$ was obtained in the present work.

## 5. Conclusions

The liquid–solid reaction between Sn–Pd alloy and Ni was found to be dominated not only by the Pd concentration but also the reaction time. $Ni_3Sn_4$ and $(Pd,Ni)Sn_4$ were the two predominant intermetallic compounds observed, which grew at the interface either separately or simultaneously depending on two factors (i.e., the Pd concentration and the reaction time). When the Pd concentration of the Sn–Pd alloy was low, e.g., 0.05 wt.%, only $Ni_3Sn_4$ was observed after reacting at 250 °C for 120–1200 s. When the Pd concentration increased to 0.1 wt.% and the reaction time was relatively short (60–150 s), discontinuous $(Pd,Ni)Sn_4$ grains scattered above the $Ni_3Sn_4$ layer were produced. Interestingly, most of the $(Pd,Ni)Sn_4$ grains disappeared, but the $Ni_3Sn_4$ remained after 300 s. When the Pd concentration further increased to 0.2 wt.% or higher, $(Pd,Ni)Sn_4$ developed as a continuous layer in contact with the $Ni_3Sn_4$.

The mechanical properties of the Sn–Pd/Ni joints were also rather sensitive to the Pd concentration, as demonstrated by the HSBS test. It was found that the shear strength dramatically degraded when the Pd concentration was equal to or greater than 0.2 wt.%, and the formation of the $(Pd,Ni)Sn_4$–$Ni_3Sn_4$ dual layer was the root cause of this degradation. The results of this study indicate that the Pd concentration has a significant influence on the Sn–Pd/Ni reaction. The Pd concentration in the Sn–Pd joints should be reduced to prevent the dual-layer structure of $(Pd,Ni)Sn_4$–$Ni_3Sn_4$ from being established at the interface.

## Acknowledgments

This study was supported by the National Science Council (R.O.C.) and Taiwan Uyemura Co., Ltd. through Grant nos. NSC99-2221-E-155-017 and NSC99-2622-E-155-008-CC3. The authors would also like to acknowledge Nico Lee (Taiwan Uyemura Corp. Ltd.) and Linda Huang (Schmidt Scientific Taiwan Ltd.) for their assistance in the experimental work.

## References

[1] H. Roberts, K. Johal, Lead-Free Soldering, Springer Press, New York, 2007 (Chapter 9).
[2] B. Kao, M. Oezkoek, H. Roberts, Proceedings of the 5th International Microsystems Packaging Assembly and Circuits Technology (IMPACT) Conference and International 3D IC Conference, 20–22 Oct, 2010, Taipei, Taiwan, 2010 (article number: 5699489).
[3] K.N. Tu, Solder Joint Technology: Materials, Properties, and Reliability, Springer Press, New York, 2007.
[4] Y.W. Yen, P.H. Tsai, Y.K. Fang, S.C. Lo, Y.P. Hsieh, C. Lee, J. Alloys Compd. 503 (2010) 25–30.
[5] J.W Yoon, B.I. Noh, J.H. Yoon, H.B Kang, S.B Jung, J. Alloys Compd. 509 (2011) 153–156.
[6] K. Zeng, R. Stierman, D. Abbott, M. Murtuza, JOM 58 (2006) 75–79.
[7] K. Suganuma, K.S. Kim, JOM 60 (2008) 61–65.
[8] P.T. Vianco, Circuit World 25 (1998) 6–24.
[9] P.G. Kim, K.N. Tu, D.C. Abbott, J. Appl. Phys. 84 (1998) 770–775.
[10] G. Ghosh, J. Electron. Mater. 28 (1999) 1238–1250.
[11] S.P. Peng, W.H. Wu, C.E. Ho, Y.M. Huang, J. Alloys Compd. 493 (2010) 431–437.
[12] K. Masui, M. Kajihara, J. Alloys Compd. 485 (2009) 144–149.
[13] J. Vizdal, A. Kroupa, J. Popovic, A. Zemanova, Adv. Eng. Mater. 8 (2006) 164–176.
[14] C.E. Ho, W. Gierlotka, S.W. Lin, J. Mater. Res. 25 (2010) 2078–2081.
[15] BGA Ball Shear, JESD22-B117, JEDEC Solid State Technology Association, edition: October 2006.
[16] K. Zeng, K.N. Tu, Mater. Sci. Eng. R38 (2002) 55–105.
[17] T. Laurila, V. Vuorinen, J.K. Kivilahti, Mater. Sci. Eng. R49 (2005) 1–59.
[18] C.E. Ho, S.C. Yang, C.R. Kao, J. Mater. Sci.: Mater. Electron. 18 (2007) 155–174.
[19] Y.C. Chan, M.Y. Chiu, T.H. Chung, Z. Metallkde 93 (2002) 95–98.
[20] C.Y. Chou, S.W. Chen, Y.S. Chang, J. Mater. Res. 21 (2006) 1849–1856.
[21] S. Bader, W. Gust, H. Hieber, Acta Metall. Mater. 43 (1995) 329–337.
[22] S. Tanaka, M. Kajihara, J. Alloys Compd. 484 (2009) 273–279.
[23] C.E. Ho, Y.W. Lin, S.C. Yang, C.R. Kao, D.S. Jiang, J. Electron. Mater. 35 (2006) 1017–1024.
[24] H.K. Kim, K.N. Tu, P.A. Totta, Appl. Phys. Lett. 68 (1996) 2204–2206.
[25] C.Y. Liu, H.K. Kim, K.N. Tu, P.A. Totta, Appl. Phys. Lett. 69 (1996) 4014–4016.
[26] H.K. Kim, K.N. Tu, Phys. Rev. B 53 (1996) 16027–16034.
[27] K. Zeng, Report on the 6th Annual Topical Research Conference on Reliability, Austin, TX, U.S.A., 2003.
[28] C.P. Lin, C.M. Chen, Microelectron. Reliab. (2011), doi:10.1016/j.microrel.2011.03.007.
[29] C.E. Ho, R. Zheng, G.L. Luo, A.H. Lin, C.R. Kao, J. Electron. Mater. 29 (2000) 1175–1181.
[30] A.M. Minor, J.W. Morris Jr., Metall. Mater. Trans. 31A (2000) 798–800.
[31] S.C. Yang, C.C. Chang, M.H. Tsai, C.R. Kao, J. Alloys Compd. 499 (2010) 149–153.
[32] W.H. Wu, H.L. Chung, B.Z. Chen, C.E. Ho, J. Electron. Mater. 39 (2010) 2653–2661.